ACS central science

Research Article

http://pubs.acs.org/journal/acscii

# Multimodal Hydrogel-Based Platform To Deliver and Monitor Cardiac Progenitor/Stem Cell Engraftment

Alessondra T. Speidel,[†,‡,⊥] Daniel J. Stuckey,[†,‡,⊥,#] Lesley W. Chow,[‡,§,∥] Laurence H. Jackson,[#] Michela Noseda,[†,⊥] Marta Abreu Paiva,[†,⊥] Michael D. Schneider,[*,†,⊥] and Molly M. Stevens[*,†,‡,§,∥]

[†]British Heart Foundation Centre of Research Excellence, [‡]Department of Materials, [§]Department of Bioengineering, [∥]Institute for Biomedical Engineering, and [⊥]National Heart and Lung Institute, Imperial College London, London, SW7 2AZ, United Kingdom

[#]Centre for Advanced Biomedical Imaging (CABI), University College London, London WC1E 6DD, United Kingdom

Supporting Information

**ABSTRACT:** Retention and survival of transplanted cells are major limitations to the efficacy of regenerative medicine, with short-term paracrine signals being the principal mechanism underlying current cell therapies for heart repair. Consequently, even improvements in short-term durability may have a potential impact on cardiac cell grafting. We have developed a multimodal hydrogel-based platform comprised of a poly(ethylene glycol) network cross-linked with bioactive peptides functionalized with Gd(III) in order to monitor the localization and retention of the hydrogel in vivo by magnetic resonance imaging. In this study, we have tailored the material for cardiac applications through the inclusion of a heparin-binding peptide (HBP) sequence in the cross-linker design and formulated the gel to display mechanical properties resembling those of cardiac tissue. Luciferase-expressing cardiac stem cells (CSC-Luc2) encapsulated within these gels maintained their metabolic activity for up to 14 days in vitro. Encapsulation in the HBP hydrogels improved CSC-Luc2 retention in the mouse myocardium and hind limbs at 3 days by 6.5- and 12- fold, respectively. Thus, this novel heparin-binding based, Gd(III)-tagged hydrogel and CSC-Luc2 platform system demonstrates a tailored, in vivo detectable theranostic cell delivery system that can be implemented to monitor and assess the transplanted material and cell retention.

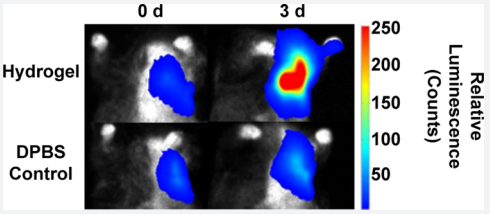


## 1. INTRODUCTION

With the advent of stem cell therapy, the regenerative medicine field united around cell transplantation as an immediately workable solution to restore damaged heart tissue. Various cell populations have been studied both preclinically and clinically, eliciting encouraging functional improvements and beneficial remodelling in the infarcted heart.[1,2] However, overall improvements in cardiac function have been at best moderate, with some metanalyses of trials reporting overall increases in ejection fraction less than 5%,[3] and other analyses of studies using the same cell type finding no improvement in contractile function.[4] The poor performance has been attributed to low donor cell retention, which when reported, is already less than 10% after 24 h.[5,6] In order to improve the efficacy of cell therapy, the field has transitioned toward developing strategies to enhance transplanted cell engraftment. Various methods, including pretreatment of transplanted cell populations and target tissue, have been attempted to achieve a sustained regenerative effect,[7,8] but the principal focus has been on developing biomaterial delivery systems to improve grafted cell viability and retention within the area of injury after myocardial infarction (MI). Biomaterials implemented in cardiac tissue engineering applications include natural materials, such as collagen,[9] alginate,[10] chitosan,[11] decellularized ECM,[12] and fibrin,[13] as well as synthetic materials, including poly(lactic-*co*-glycolic acid),[14] poly(ethylene glycol) (PEG),[15] poly(*N*-isopropylacrylamide) (pNIPAM),[16] and self-assembling peptides.[17] Although numerous combinations of materials and cellular products have been examined for their impact on cardiac regeneration after MI, progression has been limited with only three alginate-based hydrogel designs in clinical application.[18]

With the growing consensus that paracrine effects rather than direct regeneration from the grafted cells drive the observed improvements in cardiac function, interest in developing therapies that mimic or enhance this paracrine action has increased.[19,20] Superior biomaterial designs and a deeper understanding of their interactions with cells and body tissues are needed. While the retention of encapsulating biomaterial has been suggested to impact transplanted cell retention,[21] the ideal retention and degradation times of materials for optimal clinical impact are unclear and are likely to vary depending on the composition of the proposed material and its cargo.[22] The ability to monitor the retention of the biomaterial and examine its impact on cell viability and retention in vivo would provide critical information for future designs. In vivo imaging techniques such as fluorescence imaging,[23] ultrasound,[24] and optical coherence tomography (OCT)[25] have been implemented to monitor in vivo degradation of scaffold materials; however the limited tissue permeation of these detection strategies restricts their application to shallow body tissues. As

**Received:** January 23, 2017
**Published:** March 30, 2017






DOI: 10.1021/acscentsci.7b00039
ACS Cent. Sci. 2017, 3, 338−348

magnetic resonance imaging (MRI) sets the gold standard for cardiac imaging, due to its precision and permeation potential, some studies have made use of MRI-traceable probes to track the persistence of hydrogels in myocardial tissue.[26,27]

The ability to monitor the retention and viability of transplanted cells in host tissue can also provide further insight into the necessary timing, impact, and mechanisms behind their regenerative effects. A variety of cellular imaging strategies have been implemented to monitor transplanted cells' location and retention, including direct cell labeling with paramagnetic nanoparticles for MRI[28] or radioactive molecules for PET and SPECT.[29] However, these approaches cannot distinguish live from dead cells and their signals are diluted with cell division. Cell engineering with noninvasive, assayable reporter genes (e.g., fluorescence, bioluminescence, MRI, and PET/SPECT)[30] only track live cells as their detection requires metabolic activity.[31] In the preclinical setting, the luciferin-luciferase enzymatic bioluminescent reaction offers a simple and sensitive method for semiquantitative assessment of cell retention in vivo.[32]

In this work, we have developed an injectable hydrogel-based platform and conducted initial proof of concept studies in order to provide tailorable tissue regenerative options targeted toward eventual heart repair applications. Hydrogel-based biomaterials are soft injectable gels known to swell in water and can be tailored to display degradation, mechanical, biochemical, and other properties that are desirable for cardiac regenerative applications.[33] Our hydrogel design is composed of 4-arm PEG-acrylate cross-linked with heparin-binding peptides through a Michael addition with the thiol groups of the terminal cysteines. The heparin-binding sequence is LRKKLGKA, a Cardin-Weintraub consensus sequence found through screening many heparin-binding domains of proteins,[34] and has been shown to improve the delivery of growth factors and promote angiogenesis in the presence of heparin.[35] The heparin-binding peptides were further functionalized with a Gd(III)-loaded chelator to monitor the localization and retention of the hydrogel system in vivo through MRI detection strategies. Finally, the retention of luciferase-2 transduced cardiac progenitor cells within the hydrogels was monitored serially using bioluminescence imaging. This system presents a novel design that can provide the possibility to monitor both biomaterial retention and cell engraftment in vivo, informing the optimal hydrogel formulation for effective stem cell delivery to the heart.

## 2. RESULTS

**2.1. Rheology of 10% (w/v) PEG Hydrogels.** The cross-linking time and mechanical properties of the various hydrogel designs were examined through rheological techniques to ensure the feasibility of an injectable hydrogel system and similarity in their behavior with that of mouse cardiac tissue.[36] Time sweeps revealed that gel formulations containing 25%, 75%, and 100% heparin-binding peptide (HBP) cross-linking moieties had similar cross-linking times at 40 ± 2, 47 ± 4, and 39 ± 4 min, respectively. 50% HBP cross-linked gels were slightly slower at 52 ± 10 min, whereas 0% HBP cross-linked gels reached the gelation point more rapidly at 20 ± 2 min (Figure 1A).

From previous rheological optimization, a 10% (w/v) PEG concentration was determined to be the ideal base formulation based on proximity to desired moduli values displayed by healthy mouse heart tissue[36] (data not shown). Consistent

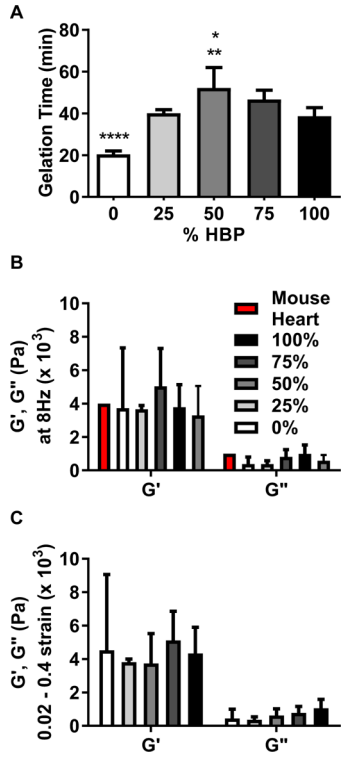


**Figure 1.** HBP hydrogel mechanical properties. Rheological profiles of 10% (w/v) PEG hydrogels: 4-arm PEG acrylate 0%, 25%, 50%, 75%, and 100% HBP hydrogels at 37 °C. (A) Mean gelation times at fixed 1 Hz and fixed 0.0001 strain in minutes. (B) HBP hydrogel mean storage modulus ($G'$) and loss modulus ($G''$) compared with literature values for mouse heart tissue from frequency sweeps at 8 Hz, fixed 0.01 strain, and (C) HBP hydrogel mean storage modulus ($G'$) and loss modulus ($G''$) from strain sweeps at 0.02−0.4 strain, fixed 8 Hz. Error bars represent one standard deviation, $*p < 0.05$ comparison with 25% HBP, $**p < 0.001$ comparison with 100% HBP, $****p < 0.0001$ comparison with 25%, 50%, 75%, and 100% HBP.

mechanical properties were displayed across the frequency range 1−10 Hz, including the frequencies of human and murine heartbeats, 1 and 8 Hz, respectively. At 8 Hz, a fixed strain amplitude of 0.01 (1%) and 37 °C, the examined hydrogel formulations displayed storage ($G'$) and loss ($G''$) moduli near the literature values of healthy mouse heart tissue, 4000 and 1000 Pa, respectively.[36] The hydrogel formulations displayed similar storage ($G'$) and loss ($G''$) moduli across 0.02−0.4 strain, a range encompassing the strains seen in remote healthy, border zone and infarct myocardial tissue. Substituting HBP for 25−100% of the cross-linkers within the PEG hydrogels caused no substantive change in the average moduli displayed in the frequency and strain sweeps at physiologically relevant conditions[37−39] (Figure 1B,C). Representative time, frequency, and strain sweeps for the 10% (w/v) HBP hydrogel formulations can be found in Supplementary Figures 6−8.

**2.2. Degradation Profiles of 10% (w/v) PEG Hydrogels.** The four HBP gel formulations tested displayed drastically different degradation profiles, as characterized by swelling ratios (Figure 2A) and changes in mass loss (Figure 2B), with full degradation ranging from 3 days (100% HBP) to more than 2 weeks (0 or 25% HBP). The swelling ratios for 0% and 50% HBP gels plateaued from 1 day onward, whereas the swelling ratios of 100% and 75% hydrogels were maximal after 4 h and 3 days, respectively. The 0% HBP gel showed the least


DOI: 10.1021/acscentsci.7b00039
ACS Cent. Sci. 2017, 3, 338−348

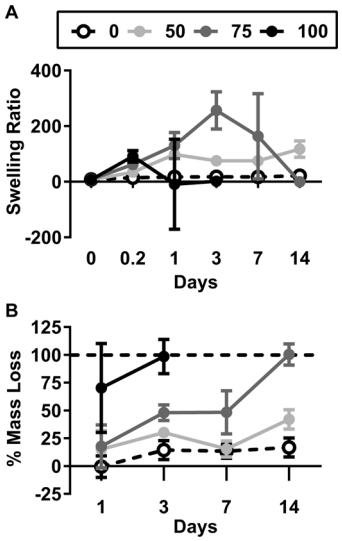


**Figure 2.** % HBP hydrogel degradation profiles. A comparison of 10% (w/v) 4-arm PEG acrylate 0%, 50%, 75%, and 100% HBP hydrogels. (A) Swelling ratios, *q*, and (B) mass loss (%) in DI water over 14 days. Error bars represent one standard deviation.

degradation over the entire 14 days (16.7% ± 8.5%). The 50% HBP gels on average lost 42% of their mass by 14 days. The 75% and 100% HBP gels were fully degraded after 14 and 3 days, respectively. The sol fractions for the 0%, 50%, 75%, and 100% HBP hydrogels were 11.7%, 12.4%, 14.8%, and 19.4%, respectively.

**2.3. MRI Measurement of 10% (w/v) PEG Gd(III) Hydrogel Degradation.** T1 signal intensity was found to correlate with Gd(III) concentration, represented by swelling ratios in two independent Gd(III)-containing hydrogel formulations examined over 7 and 14 days (Figure 3). The T1 signals (Figure 3A) and swelling ratios (Figure 3B) were examined in HBP hydrogels with and without Gd(III). The samples containing Gd(III) contained a previously optimized 2 mM equivalent of Gd(III)-HBP cross-linker substituted for HBP or dithiol cross-linkers in the 50% HBP and 40% HBP formulations, respectively (see Supplementary Figure 2). The average overall starting hydrogel mass was 29.1 ± 2.1 mg with no significant difference across the hydrogel samples (Supplementary Figure 4A). The swelling ratios of the various experimental and control hydrogels all demonstrated similar increases over time (Figure 3B). However, only the swelling ratios of 50% or 40% HBP-Gd(III) hydrogels correlated with T1 value (50% HBP − Gd(III), $r^2$ = 0.9982, 40% HBP − Gd(III), $r^2$ = 0.9213; Figure 3C) and only the 50% and 40% HBP Gd(III)-containing hydrogels showed linear correlations between T1 intensity and time ($r^2$ = 0.9380 and $r^2$ = 0.9180, respectively; Figure 3D). The incorporation of Gd(III)-tagged HBP did not appear to influence the degradation of the hydrogels, as demonstrated by similar swelling ratio changes over time demonstrated between the experimental Gd(III)-containing and control samples (Figure 3B).

**2.4. Impact of HBP on CSC Durability in Hydrogels.** After it was determined that the 50% HBP hydrogel formulation exhibited the lowest amount of degradation over 14 days (Figure 2) and demonstrated mechanical properties resembling those of mouse cardiac tissue (Figure 1), the potential benefit of this HBP-containing hydrogel formulation was tested by monitoring the luciferase activity of encapsulated CSC, a noninvasive serial measurement that reflects the

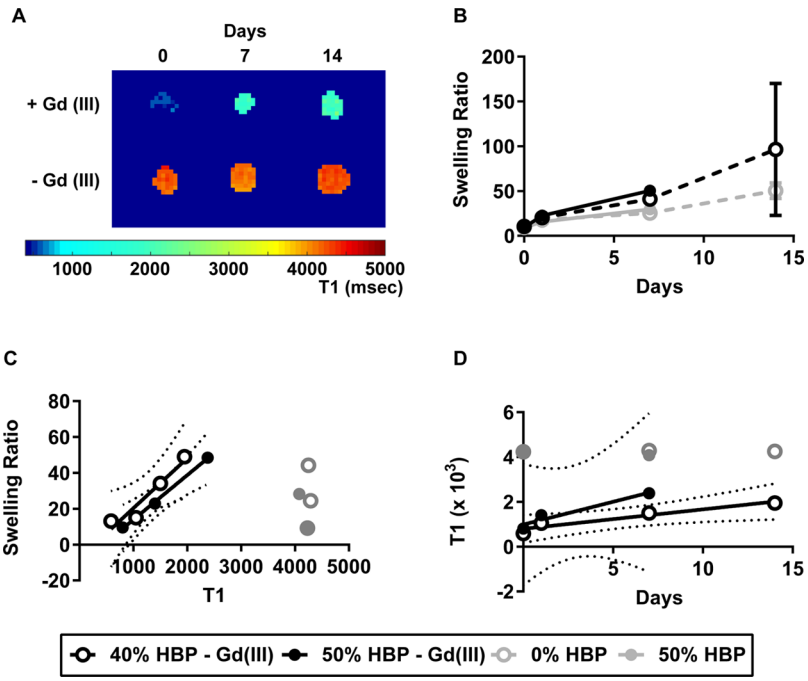


**Figure 3.** Correlation of Gd(III)-containing hydrogel degradation and T1 in vitro. (A) Representative T1 images of Gd(III)-containing and control hydrogel samples. (B) Distribution of measured swelling ratios across samples and time points. Error bars represent one standard deviation. (C) Representative swelling ratio and T1 correlations (50% HBP − Gd(III), $r^2$ = 0.9982, 40% HBP − Gd(III), $r^2$ = 0.9213). (D) Representative T1 value correlation with degradation time points (days) (50% HBP − Gd(III), $r^2$ = 0.9380, 40% HBP − Gd(III), $r^2$ = 0.9180). T1 units are all in milliseconds. Sample T1 values decrease with higher Gd(III) concentration. 95% CI are designated by black dotted lines and were included for experimental samples where $r^2$ of correlation was above 0.90.



DOI: 10.1021/acscentsci.7b00039
*ACS Cent. Sci.* 2017, 3, 338−348

number of viable, metabolically active cells in vitro and in vivo[40] (Figure 4). The initial number of inoculated CSC-Luc2 cells

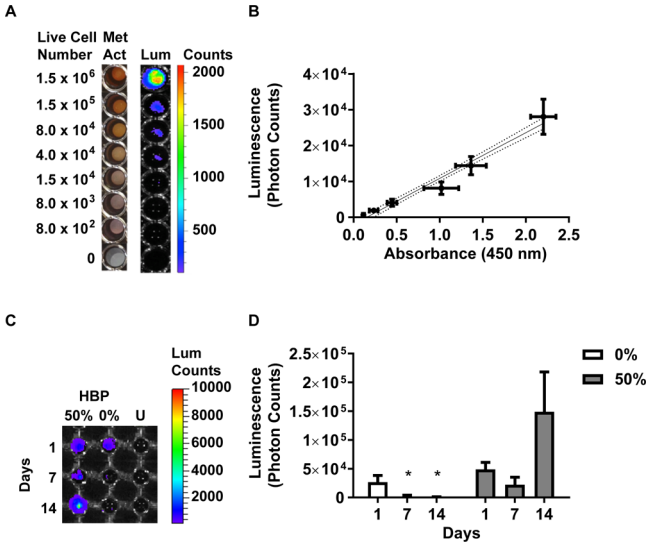


**Figure 4.** Metabolic activity of CSC-Luc2 in 10% (w/v) 4-arm PEG acrylate 0% and 50% HBP hydrogels. (A) CSC-Luc2 luminescent activity correlation to metabolic activity validation images of representative CCK-8 metabolic activity assay and luminescent counts of CSC-Luc2 seeded at various densities from $1.5 \times 10^6$ through $8.0 \times 10^2$. (B) The correlation of the average luminescent activity (photon counts) and absorbance (450 nm) of CSC-Luc2 densities below $10^5$ can be approximated linearly ($r^2 = 0.9182$). Error bars represent one standard deviation ($n = 9$). Solid line represents best linear fit ($r^2 = 0.9182$) and dotted lines represent 95% CI. (C) Image of luminescent counts of representative CSC-Luc2 in 50% and 0% HBP hydrogels and untransduced controls at days 1, 7, and 14. Luminescence used as a corollary to metabolic activity. (D) Mean luminescence in photon counts of CSC-Luc2 in 0% and 50% HBP gels. Bioluminescent images taken on IVIS software. Error bars represent standard error. Samples compared by one-way ANOVA, Bonferroni's multiple comparison test, $*p < 0.05$ in comparison with Day 1.

encapsulated in hydrogels was similar between the 0% and 50% HBP gels (Supplementary Figure 5), excluding variation in the luciferase signals from inadvertent mere differences in initial seeding density. In 50% HBP gels, the cells' luciferase activity persisted for at least 14 days, but in 0% HBP gels, cells' luciferase activity was undetectable even at 7 days (Figure 4). Thus, the inclusion of 50% HBP markedly prolonged CSC-Luc2 viability in vitro, compared with HBP-free hydrogels.

**2.5. Engraftment of CSC in 50% and 100% HBP Hydrogels in Mouse Hind Limb Injections.** In order to assess whether the differences observed in the in vitro degradation of the HBP hydrogels were predictive of the gels' persistence and encapsulated CSC retention in vivo, hind limb injections of 100% and 50% HBP-Gd(III) were made and compared with unencapsulated control cells over 14 days. These two hydrogel formulations were selected due to their differences in HBP content and because they displayed the most significantly different degradation profiles — 100% HBP fully degrading within 3 days and 50% HBP degrading only 42% over 14 days (Figure 2). The aggregate photon signals from the samples were collected over 20 min, and serial determinations were normalized to the starting value for each animal.

At 3 days, compared to control sites with CSC-Luc2 cells merely injected in DPBS, CSC-Luc2 injections in 50% or 100% HBP-containing gels demonstrated 12- and 13-fold higher bioluminescent signals, respectively ($p < 0.0001$; Figure 5).

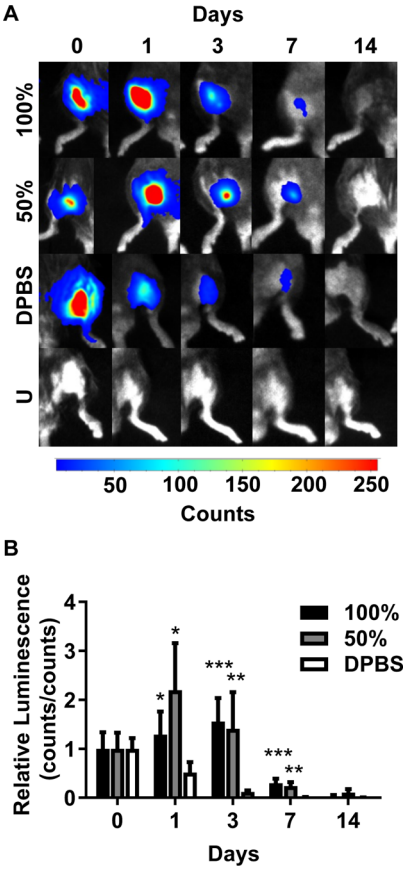


**Figure 5.** CSC-Luc2 retention in mouse hind limbs. (A) Representative bioluminescent images of intramuscular hind limb injections of $1.5 \times 10^6$ CSC-Luc2 in 100%, 50% HBP hydrogels containing 2 mM Gd(III) and DPBS. (B) Mean relative luminescent counts at days 1, 3, 7, and 14 relative to day 0 in hind limbs. Data represented as luminescent photon counts normalized to day 0 photon counts. Error bars represent standard error; $*p < 0.05$, $**p < 0.01$, $***p < 0.001$ in comparison with DPBS.

There was no difference in CSC retention between the 50% and 100% gel formulations. At 7 days, though much of the luminescent signal had subsided, the 50% and 100% HBP-containing gels still retained an 18- and 23-fold higher signal, respectively, versus CSC-Luc2 cells injected in DPBS ($p < 0.0001$). Under the conditions tested, little signal remained at 14 days. T1 mapping of the mouse hind limbs revealed that no hydrogel material was left at day 7 or 14.

**2.6. Engraftment of CSC in 50% HBP Hydrogels in Mouse Ultrasound-Guided Intramyocardial Injections.** Given the equal performance of 50% and 100% HBP hydrogels in the enhancement of CSC hind limb retention, ultrasound-guided intramyocardial injections were conducted to determine if the 50% HBP hydrogel likewise improved intramyocardial retention. The intramyocardial injection of HBP hydrogel did not appear to evoke any immediate adverse effects on cardiac pump function (Supplementary Figure 9). The 50% HBP demonstrated enhanced CSC-Luc2 retention 6.5-fold at 3 days compared to cells injected in DPBS ($p = 0.0028$; Figure 6). At 7


DOI: 10.1021/acscentsci.7b00039
ACS Cent. Sci. 2017, 3, 338−348

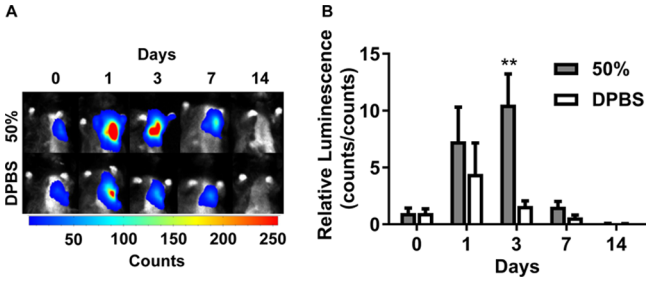


**Figure 6.** CSC-Luc2 retention in mouse myocardium. (A) Representative images of CSC-Luc2 retention after ultrasound-guided intramyocardial injections $4 \times 3.5 \times 10^5$ CSC-Luc2 in 50% HBP hydrogels containing 2 mM Gd(III) and DPBS. (B) Mean luminescent counts at days 1, 3, 7, and 14 relative to day 0 in heart. Data represented as luminescent photon counts normalized to day 0 photon counts. Error bars represent standard error, $^{**}p < 0.01$ in comparison with DPBS.

days, CSC engraftment was enhanced 2.6-fold by 50% HBP ($p = 0.0564$), at the threshold of statistical significance. T1 mapping of the mouse chests revealed that no hydrogel material was left at day 7 or 14.

## 3. DISCUSSION

Cell retention remains a paramount challenge for injection-based cell therapy, leading to keen interest in diverse tissue engineering approaches. Hydrogels and other delivery biomaterials can improve this retention, but the ideal tissue-appropriate formulations, degradation times,[22] and other mechanisms behind the impact of these formulations remain unclear, hindering further progress in the field. Here, we present an injectable, multimodal platform for a selection of hydrogel-based designs composed of 4-arm PEG acrylate cross-linked with PEG dithiol and heparin-binding peptides containing a Gd(III) contrast agent. These hydrogels provide the possibility to be monitored in vivo and tailored to deliver cellular cargo, in order to address these open questions. MRI-sensitive-Gd(III) conjugated peptides have been implemented for tumor-tracking[41] and comparison of biomaterial degradation,[42] but here we present a Gd(III)-tagged peptide platform system that can be easily incorporated into commonly implemented and easily functionalized PEG-based hydrogels for imaging biomaterial carriers for cell delivery in cardiac cell therapy applications.

In the clinical context of acute MI, many of the biomaterials examined for encouraging cellular retention—including many variations of an epicardial patch—have limited applicability due to the necessity, safety, or preference for delivery via a catheter.[43] Conversely, the clinical application of many current injectable hydrogel systems is hampered by rapid gelation rates, making catheter delivery logistically challenging or impossible.[43] In the present study, the 0% HBP hydrogels had significantly faster cross-linking times compared with the HBP-containing formulations. The bulky, charged side chains in the HBP peptides may create steric and repulsive interactions that slow the cross-linking process in the HBP-containing gels compared with the smaller, uncharged simple PEG dithiol cross-linkers used in the 0% HBP hydrogels. The hydrogel formulations containing HBP took approximately 40−50 min to reach their gelation points (Figure 1A), providing a convenient time window for preparation of the cell-hydrogel injection suited to clinical applications as the hydrogel components can be mixed and the cross-linking process can begin before the hydrogel system is injected in vivo. This longer gelation time creates an experimental setup that provides workable advantages over the rapid gelation times seen in alginate systems, the only biomaterial currently in clinical trials for cardiac applications.

It is well-known that the mechanical properties of a cell's environment can impact cell behavior, and, in the cardiac context, the remodelling and changes in cardiac tissue mechanical properties can contribute to the progression of heart failure. Thus, the mechanical properties of the encapsulating hydrogel formulation were tailored to recapitulate the properties of native cardiac tissue.[36] The moduli of the gel formulations were easily manipulated through altering the concentration of the base hydrogel system, and a 10% (w/v) concentration was determined to be the most desirable across all % HBP formulations, displaying storage ($G'$) and loss ($G''$) moduli resembling those values present in mouse heart tissue[36] (Figure 1B). The various % HBP formulations demonstrated consistent moduli, exhibiting the ability to maintain mechanical properties, across the range of strains seen in remote healthy (0.028−0.33 strain),[37] infarct (0.027−0.15 strain),[37] and border zone (0.09 peak strain) myocardium[39] (Figure 1C, Supplementary Figure 8).

The desired timing of biomaterial degradation for optimal clinical impact is unknown; thus creation of a panel of hydrogel formulations with varying degradation rates presents a valuable means for exploring and clarifying this question. The various HBP-containing hydrogel formulations displayed a spectrum of degradation profiles ranging from full degradation in 3 days to only 42% mass loss over 14 days (Figure 2). The HBP sequences included within the hydrogel design are not designed to degrade and do not contain any known proteolytic degradation sequences. However, the termini of the PEG arms within the hydrogel design implemented in these studies are modified with acrylate groups that react with the thiol termini of the cross-linking HBP peptides and/or PEG dithiol through Michael addition to form relatively unstable ester bonds susceptible to degradation through hydrolysis,[44,45] a process accelerated in basic environments.[44] HBP is faintly positive in charge (Supplementary Table 1); thus water, as a polar molecule, is likely attracted to the charged components of the hydrogel system causing the formulations with higher densities of these bulky positively charged moieties to swell more quickly. Comparing the swelling ratios of the various hydrogel formulations (Figure 2A), the higher percentage of HBP cross-linkers within the hydrogel formulation correlated with more rapid swelling of the hydrogels. 100% HBP reached its peak swelling ratio of 91.2 ± 21.1 after 4 h, 75% HBP was 256 ± 66 after 3 days, while at 14 days 50% and 0% HBP exhibit values of 117 ± 30 and 21.9 ± 2.7, respectively (Figure 2A). The faster swelling formulations also appear to degrade the most rapidly (Figure 2), likely due to increased water content within the hydrogels, increasing exposure of the ester bonds to hydrolysis. Because of the diversity of hydrogel amounts and volumes remaining over the diverse degradation time courses examined across the various hydrogel formulations, it was difficult to meaningfully measure and compare the impact of hydrogel degradation on hydrogel mechanical properties.

To examine the impacts of this degradation behavior in vivo, MRI-detectable HBP peptides containing MRI-sensitive Gd(III) were incorporated into the hydrogel design. The T1 signal


DOI: 10.1021/acscentsci.7b00039
ACS Cent. Sci. 2017, 3, 338−348

of independent formulations of 40% and 50% HBP hydrogels demonstrated nearly identical dependence on Gd(III) concentration, represented by the swelling ratio (Figure 3B−C). The sensitivity of this hydrogel system to the changes in Gd(III) concentration over time demonstrates the potential to monitor the tagged hydrogel degradation in vivo over time.

Before in vivo application, the impact of 50% HBP, the most persistent hydrogel formulation, on CSC metabolic activity was examined in vitro. CSC luciferase activity, a surrogate measurement of metabolically active cells, remained consistent in HBP-containing gels, but diminished over 14 days when encapsulated in hydrogels without HBP (Figure 4). The improved viability of the CSC in the HBP-containing gels may result from the HBP moiety attracting heparin-bound regenerative factors from the local milieu[46,47] to the encapsulated cell populations within the hydrogel. The increased swelling ratio of the 50% HBP hydrogel may also facilitate diffusion and delivery of these factors as well as provide space for cell proliferation compared with the 0% HBP hydrogels. The tailored mechanical properties of both hydrogel formulations to match those of native cardiac tissue appear to be insufficient for maintaining the metabolic activity of the cells within the 0% HBP formulations, but may contribute to the maintained metabolic activity observed in the 50% HBP hydrogels. The consistent preservation of CSC within the 50% HBP compared with the reduction seen in the 0% HBP reached statistical significance at 7 days, demonstrating that the presence of HBP enables cell survival. Thus, in vitro the 50% HBP hydrogel exhibits the most desirable combination of mechanical properties (Figure 1), degradation properties (Figure 2), and ability to support viable, metabolically active cells (Figure 4).

In vivo, the 50% and 100% HBP hydrogels, with significantly different in vitro degradation profiles, were compared with DPBS and examined for their impact on encapsulated CSC-Luc2 retention in hind limb injections. CSC-Luc2 encapsulated in 50% or 100% HBP display enhanced bioluminescent signal after hind limb injection that is 12- and 13-times and 18- and 23-times higher than the signal produced by the samples injected with CSC-Luc2 in DPBS, after 3 and 7 days, respectively. No statistically significant differences in the bioluminescent signal exist between the 100% and 50% gel formulations despite their in vitro differences in degradation. Previous work has shown that the longer a delivery biomaterial resides in the target tissue, the higher the retention of delivered cells.[21] Interestingly, our data show that both 100% and 50% HBP formulations behaved similarly, with an improvement in cell retention in both formulations after 3 days when compared to the DPBS injected cell sites (Figure 5), and the T1 mapping of the mouse hind limbs performed at days 7 and 14 revealing that there was no detectible Gd(III) signal in any of the hydrogel formulation treated regions. These results suggest that the degradation profile of the 50% HBP hydrogel system in vivo is likely more rapid than predicted by the in vitro data. This inability to detect material from either hydrogel formulation at 7 days correlates with the cell retention data. The similarity in cell retention between hydrogel formulations could also suggest that the presence of the bioactive HBP present in both hydrogel formulations might be a more dominant force behind the observed enhancement. Taken with the ability of the 50% HBP hydrogel to maintain CSC metabolic activity compared with the 0% HBP controls (Figure 4), it is possible that the ability of the HBP moieties to attract heparin-bound regenerative factors may provide enhanced CSC metabolic activity or proliferation in the 100% HBP hydrogels compared with the 50% HBP hydrogels that may enable the encapsulated CSC to remain engrafted at a similar level to those in the 50% HBP. However, as luciferase activity has been shown to correlate with both cell number and the metabolic activity of cells, its persistence in cell delivery studies cannot be interpreted simplistically. Further examination of more persistent hydrogel formulations of our tunable platform system could further distinguish the impact of these possible mechanisms on the observed cell retention data.

In intramyocardial injections, a similar cell retention pattern was observed at 3 days with an increased viable CSC population observed in the sites where cells were injected in the 50% HBP formulation compared to DPBS (Figure 6) with a relative luminescent signal ∼6.5 times higher compared to that exhibited by CSC-Luc2 injected in DPBS. Similar to the hind limb injections, MRI imaging of the mouse chests revealed that no hydrogel material remained at day 7 or 14. Thus, markedly improved levels of CSC retention were demonstrated by HBP-containing gels compared with DPBS controls in both hind limb and intramyocardial injections at 3 days, notably higher than the enhancement of cell retention by other PEG-based hydrogel designs at comparable early time points.[48,49] In one of these studies, a PEGylated-fibrinogen hydrogel encapsulating neonatal rat ventricular cardiomyocytes (NRVCM) was found to enhance cell retention within the heart ∼2.5 times over saline injected controls after 2 days.[49] In rats with MI, this hydrogel system and encapsulated NRVCM were found to improve cardiac function and remodelling after 30 days when compared with saline, NRVCM only, and PEGylated-fibrinogen only controls.[49] Although our studies were conducted in healthy mice, the fact that our hydrogel system retained over twice as many cells compared with this study at a time point a day later is encouraging for considering the impact of our system on cardiac function, remodelling, and structure for treatment post-MI.

## 4. CONCLUSIONS

In summary, we have designed and characterized a tailored and in vivo detectable Gd(III) HBP hydrogel system that displays mechanical properties resembling cardiac tissue and maintains cell metabolic activity while delivering CSC. This platform system provides a collection of hydrogel formulations that display modulated bioactive components and an array of degradation properties. As the degradation of biomaterial systems are known to vary in their behavior in vitro and in vivo, future applications of this platform system could be tailored to further explore these variations and their implications for enhancing existing cell therapies.[50] The system also contains a well-characterized in vivo detectable cellular population with the ability to map cell location, metabolic status, and retention. Altogether, this system presents possibilities for the noninvasive ability to improve and trace viable cell and material retention in hind limbs and myocardium in vivo.

With so many current approaches in the literature turning toward the examination of combinatorial effects of materials and cellular materials on cardiac regeneration after MI,[18,43] this theranostic system provides the opportunity to dissect and better understand the individual effects of the various components of these systems and how they mechanistically work together to bestow any beneficial effects observed within the target tissue. Previous approaches focus mainly on either


DOI: 10.1021/acscentsci.7b00039
ACS Cent. Sci. 2017, 3, 338−348

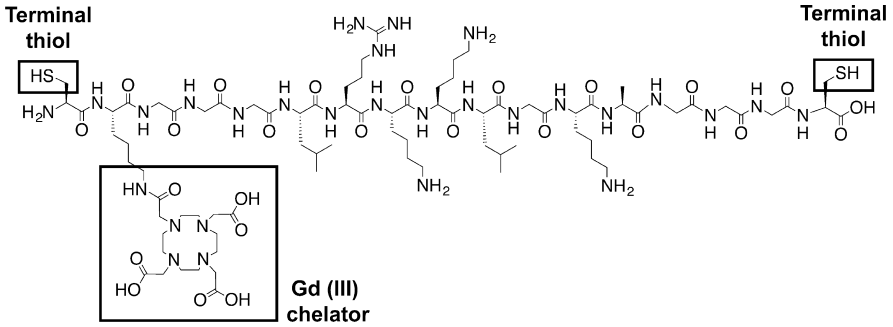


**Figure 7.** Chemical structure of synthesized peptide Gd(III) chelator HBP: CK(DOTA)GGGLRKKLGKAGGGC (MW: 1976). The peptide sequence is composed of terminal cysteines containing thiol side chains that facilitate hydrogel cross-linking and three sequential glycines for structural flexibility that flank a central heparin binding region composed of the amino acid sequence LRKKLGKA. A lysine following the terminal cysteine at the peptide's N-terminus functions to tether the Gd(III) chelator to the peptide structure. The simple HBP peptide without Gd(III) functionality is composed of an identical amino acid sequence without the additional lysine and Gd(III) chelator, CGGGLRKLGKAGGGC (MW: 1461).

the in vivo retention of material[51] or the retention of cellular material,[28] but few studies examine systems capable of effectively monitoring both. This multimodal system presents the opportunity to assemble and organize much of the seemingly competing, disconnected, and widely diverse array of work attempting to address the problem of cardiac regeneration[43] and design noninvasive, tailored in vivo therapies that address the various remaining major design questions and challenges facing cell therapy trials, such as optimal dosage, delivered cells, and material retention times.[5] The applications of this careful, yet powerful, strategy and multimodal platform system are flexible and can be optimized, not just in an MI model, but across all tissue engineering and drug delivery applications.

## 5. MATERIALS AND METHODS

**5.1. Peptide Synthesis.** Amino acids were purchased from AGTC Bioproducts Ltd. (Hessle, UK), except for Fmoc-Cys(tBU)-OH which was purchased from Novabiochem (Merck, Darmstadt, DE) and used without further purification. Peptides were synthesized on a RINK amide MBHA resin (AGTC Bioproducts Ltd., Hessle, UK) by standard Fmoc solid-phase peptide synthesis. Briefly, Fmoc-protected amino acids were coupled through successive additions of a 4-molar excess amino acid, 6-molar excess diisopropylethylamine (Sigma, Dorset, UK), and 3.95-molar excess 2-(1*H*-benzotriazole-1-yl)-1,1,3,3-tetramethyluronium hexafluorophosphate (HBTU; AGTC Bioproducts Ltd., Hessle, UK) in dimethylformamide (DMF; AGTC Bioproducts Ltd., Hessle, UK). Each coupling reaction was allowed to proceed for at least 2−3 h and then washed with DCM and DMF. Before each coupling, Fmoc protecting groups were removed with 20% (v/v) piperidine in DMF and were washed with DCM and DMF. Nihydrin tests were performed to monitor the presence of free amines after each Fmoc deprotection and coupling step. The partial HBP peptide sequence GGGLRKKLGKAGGGC (MW: 1357) was synthesized on a Quartet multiple synthesizer (Protein Technologies Inc., Tucson, AZ). The product was split into two batches, from which the complete HBP peptide (CGGGLRKKLGKAGGGC; MW: 1461) and Gd chelator-HBP peptide (CK[DOTA]GGGLRKKLGKAGGGC; MW: 1976) were manually synthesized (Figure 7). In continuing the synthesis of the Gd chelator-HBP peptide, DOTA was added orthogonally, via a Lys(Mtt), to the partial HBP peptide. Gd chelator-HBP peptide synthesis was continued with manual addition of Fmoc-Lys(Mtt)-OH; removal of the Mtt protecting groups with 2% (v/v) trifluoroacetic acid (TFA; Sigma, Dorset, UK), 93% (v/v) dicholoromethane (DCM; AGTC Bioproducts Ltd., Hessle, UK), 5% (v/v) triisopropylsilane (TIS; Sigma, Dorset, UK); and two additions of 2-molar excess 1,4,7,10-tetraazacyclododecane-1,4,7-tris-*tert*-butyl acetate-10-acetic acid (DOTA-tris (*t*-Bu ester); Macrocyclics, Dallas, TX) in an appropriately scaled previously mentioned amino acid coupling cocktail. The full-length peptides were deprotected and then cleaved from the resin using a cleavage cocktail consisting of 95% (v/v) TFA, 2.5% (v/v) micropure water, 2.5% (v/v) TIS, and 2.5% (w/v) dithiothreitol. A dichloromethane (DCM) wash was used to recover any residual peptide. TFA and DCM were then removed by rotary evaporation. The peptides were precipitated in and washed three times with cold diethyl ether and centrifuged at 6500 rpm at 4 °C for 10 min. Residual ether was decanted and the peptide samples were dried on a vacuum desiccator overnight. The peptides were redissolved in micropure water and freeze-dried. Peptide purification was performed using reverse phase preparative high performance liquid chromatography (HPLC; Shimadzu, Milton Keynes, UK) with a Phenomenex C18 Gemini NX column (150 × 21.2 mm, 5 $\mu$m pore size, 110 Å particle size). After a peptide was loaded onto the column, a gradient consisting of 5−100% (v/v) buffer B (acetonitrile with 0.1% (v/v) TFA) in buffer A (micropure water with 0.1% (v/v) TFA) was run to elute the peptide. Pure peptide was lyophilized on a freezer dryer (Labconco, Kansas City, MO), and the mass of each purified peptide was confirmed by matrix-assisted laser desorption/ionization mass spectrometry (4800 MALDI TOF/TOF, AB Sciex, Framingham, MA; Supplementary Figure 1). The synthesized peptides achieved greater than 95% purity as determined by HPLC. The final Gd-conjugated HBP peptide was prepared by mixing 17.2 mg of $GdCl_3$ (Sigma-Aldrich, Dorset, UK; MW: 371.7) to 68.66 mg of Gd chelator-HBP peptide in deionized (DI) water, pH 6.5, on rollers for 2 days and purified by dialysis in DI water for 3 days (100−500 Dialysis Membrane, Spectrum Laboratories Inc., Loughborough, UK).

**5.2. Hydrogel Formation.** The thiols of poly(ethylene glycol, PEG) dithiol (DT) (MW: 1000; Sigma-Aldrich, Dorset, UK) and the terminal cysteine groups on the heparin-binding sequence-containing peptides (HBP) were reacted with the acrylate groups of the 4-arm PEG acrylate (MW: 20,000, Laysan Bio Inc., Arab, AL) in a Michael addition[52] to form 10%


DOI: 10.1021/acscentsci.7b00039
ACS Cent. Sci. 2017, 3, 338−348

(w/v) PEG gels with varying percentages of HBP and DT cross-linkers. 100% HBP and 0% HBP (100% DT) cross-linker stock solutions were prepared by dissolving 1.461 mg of HBP peptide and 1 mg of poly(ethylene glycol) dithiol per 40 $\mu$L of DPBS, respectively. A 4-arm PEG acrylate stock solution was prepared by dissolving 10 mg of 4-arm PEG acrylate per 160 $\mu$L of Dulbecco's phosphate-buffered saline (DPBS). For gels containing cells, 160 $\mu$L of cardiac progenitor cell suspension in DPBS was added per 10 mg of 4-arm PEG acrylate. The stock solutions for 25%, 50%, and 75% HBP cross-linker were formed by mixing 10, 20, or 30 $\mu$L of 100% HBP for every 30, 20, or 10 $\mu$L of 0% HBP, respectively. The final hydrogels were formed by adding 40 $\mu$L of cross-linker solution to each 160 $\mu$L of 4-arm PEG acrylate solution.

**5.3. Rheology.** Mechanical characterization of 40 $\mu$L hydrogels for each gel formulation was performed on an AR2000Ex rheometer (TA Instruments, New Castle, DE) with 8 mm diameter soft solids tester geometry at a 500 $\mu$m gap distance. Experiments were repeated on at least three samples. All rheological sweeps were conducted at 37 °C to simulate physiological conditions. Dynamic oscillatory time sweeps of each formulation were collected at an angular frequency of 1 Hz and 0.0001 (0.01%) strain at 37 °C for at least 45 min. Frequency sweeps of 1−10 Hz ($\omega$ = 6.3−62.83 rad/s) were performed at a fixed strain amplitude of 0.01 (1%) and 37 °C. Strain amplitude sweeps from 0.004 to 4.00 (0.4−400%) strain were performed at angular frequencies of 8 Hz (52.3 rad/s) and 37 °C.

**5.4. Gel Degradation.** 50 $\mu$L gel formulations were prepared in preweighed 50 mm Petri dishes and allowed to form for 4 h at 37 °C. Hydrogel degradation profiles were assessed based on methods outlined in Mawad et al. 2007.[53] Wet masses of the hydrogels were assessed at fabrication ($m_{iw}$) and randomly selected samples for each material ($n$ = 5) were lyophilized to determine initial dry mass ($m_{id}$). Ten milliliters of DI water was added to the remaining samples, which were incubated at 37 °C. At different time points up through 14 days, at least three samples of each gel formulation were blotted dry and weighed to determine the swollen mass of the hydrogels ($m_s$). The hydrogels were then lyophilized overnight and weighed to obtain the dry mass of the remaining hydrogel ($m_d$).

The initial dry mass ($m_{id\_calc}$) for each hydrogel was calculated by multiplying $m_{iw}$ of individual hydrogels by the average of the initial dry masses divided by the initial wet mass of the samples assessed immediately after fabrication ($m_{id}/m_{iw}$).

The sol fraction was determined as the % mass loss calculated after 4 h incubation. This sol fraction was subtracted from $m_{id\_calc}$ to give the adjusted initial polymer mass ($m_{id\_adj}$).

$$\%\text{mass loss} = \frac{m_{id_{adj}} - m_d}{m_{id_{adj}}} \times 100 \quad (1)$$

The mass swelling ratio, $q$, was determined as

$$q = \frac{m_s}{m_d} \quad (2)$$

All determinations were based on the average of at least three samples.

**5.5. T1 Mapping of Gd-Labeled Hydrogels.** 10% (w/v) PEG DT gels with 3, 2, 1, 0.5, 0.2, and 0 mM Gd(III)-HBP were fabricated in 0.2 mL PCR tubes (VWR, Lutterworth, UK). Gels were placed at 37 °C for 45 min and subsequently were imaged along with DPBS and DI water controls using a 9.4 T MRI system (Agilent, Santa Clara, USA). T1 mapping was performed using a fully relaxed look locker sequence with 80 inversion times and inversion spacing of 50 ms.[54] Data were analyzed in MATLAB (2014b, The Mathworks Inc., Natick, USA) using in-house-written scripts and is shown in Supplementary Figure 2.

**5.6. T1 Correlation with Gd(III) Hydrogel Degradation.** 40% and 50% HBP containing 2 mM Gd(III) and control hydrogels were fabricated in PCR tubes for analysis on days 0, 1, 7, and 14 ($n$ = 3 per time point, per hydrogel formulation) and were allowed to cross-link for 4 h at 37 °C. Wet masses of the hydrogels were assessed at fabrication. For the time points after day 0, DI water was added in excess and samples were incubated at 37 °C until the time point analyzed. DI water not taken up by the hydrogels was aspirated and samples were weighed to determine the swollen mass of the hydrogels ($m_s$). Representative samples for each hydrogel formulation and time point were imaged to obtain T1 maps for the various conditions tested. All samples were then lyophilized to determine dry mass ($m_d$) and the mass swelling ratio, $q$, was determined by eq 2 as above.

**5.7. CSC Culture.** Clonally derived CSC were isolated as described.[6] Briefly, hematopoietic lineage marker-negative, Sca-1 positive side population cells were cloned from adult murine hearts by preparative flow sorting and single-cell deposition. CSC were cultured in cardiosphere-growing medium (CGM) (58.5% (v/v) Dulbecco's modified Eagle's medium; 31.5% (v/v) Iscove's modified Dulbecco's medium; 6.5% (v/v) Ham's medium F12; 3.5% (v/v) bovine growth serum (BGS; Hyclone, GE Healthcare Life Sciences, Little Chalfon, UK); 0.65 X B27; 100 $\mu$g mL$^{-1}$ penicillin; 100 U mL$^{-1}$ streptomycin; 250 ng mL$^{-1}$ amphotericin; 2 mM L-glutamine; 0.1 mM 2-mercaptoethanol (Sigma-Aldrich, Dorset, UK); 6.5 ng mL$^{-1}$ recombinant human epidermal growth factor (EGF; Peprotech, London, UK); 0.52 mUv mL$^{-1}$ thrombin (Roche, West Sussex, UK); 0.65 ng mL$^{-1}$ recombinant human cardiotrophin-1 (CT-1; Cell Sciences, Canton, MA); 13 ng mL$^{-1}$ recombinant human fibroblast growth factor (FGF; Peprotech, London, UK) at 37 °C, 5% $CO_2$ on collagen I-coated tissue culture polysterene. Unless otherwise specified, all cell culture components were supplied by Invitrogen (Fisher Scientific, Loughborough, UK). For the present proof-of-concept experiments, clone 16 was used as a representative example, which is typical of the cloned CSC with respect to growth characteristics, immunophenotype, cardiogenic signature, in vivo differentiation, and in vivo benefit to infarcted myocardium.[6] The CSC were passaged at 70% confluence every 2 to 3 days by trypsinisation in 0.25% (w/v) trypsin; 1 mM ethylenediaminetetraacetic acid (EDTA). Viable cells were counted at each passage with a Vi-CELL Cell Viability Analyzer by trypan blue exclusion (Beckman Coulter, High Wycombe, UK).

**5.8. Lentiviral Luciferase Transduction and in Vitro Assays.** Luciferase lentivirus was prepared by cotransfection of HEK 293T cells with pLenti-III-PGK-Luc2 (Applied Biological Materials, Richmond, BC), together with the psPAX packaging vector and pMD2.G envelope vector (kindly provided by Didier Trono). The pLenti-III-PGK-Luc2 vector drives Luc2 expression through the ubiquitous phosphoglycerate kinase (PGK) promoter. CSC were seeded at 10 000 cells/cm$^2$ and cultured at 37 °C and 5% $CO_2$ overnight before transduction in a solution composed of 50% (v/v) 0.45 $\mu$m filtered viral supernatants and 50% (v/v) CGM in the presence of 8 $\mu$g/mL hexadimethrine bromide (Polybrene, Sigma-Aldrich, Dorset,


DOI: 10.1021/acscentsci.7b00039
ACS Cent. Sci. 2017, 3, 338−348

UK). CSC-Luc2 cells stably expressing firefly luciferase were selected for 14 days in 3 μg/mL puromycin. Black 96-well half-area clear flat bottom plates (Greiner Bio-One Ltd., Stonehouse, UK) were coated overnight at 37 °C with 20 μL hydrogels. Cells were stained with 25 μg/mL Xenolight DiR fluorescent lipophilic membrane dye (PerkinElmer, Llantrisant, UK) for 30 min at 37 °C. Three independent formulations of 0% and 50% HBP gels composed of 11.0 × $10^3$ CSC-Luc2 cells/10 μL and one control formulation of 0% HBP gel containing 19.9 × $10^3$ CSC/10 μL were seeded at least in triplicate. Hydrogel solutions were allowed to cross-link for 6 h at 22 °C before CGM was added to each well. To give a relative quantification of the seeded cell numbers, an initial fluorescence reading of the plate was taken for 1 s at excitation 740 nm/emission 790 nm using an IVIS Lumina III (In vivo Imaging System, PerkinElmer, Llantrisant, UK). 300 μg/mL D-luciferin (PerkinElmer, Llantrisant, UK) in CGM was added to each sample and aggregate photon count over 20 min was measured 2 min following the addition of D-luciferin solution at 1, 7, and 14 days. Media were added every 3−4 days. The average background fluorescence and luminescence of empty wells and untransduced samples, respectively, were subtracted from all values. Averages were taken for the 0% HBP gel containing untransduced CSC ($n \geq 5$) and three independent formulations for the 0% and 50% HBP gel formulations containing CSC-Luc2 ($n \geq 3$).

**5.9. Hind Limb Intramuscular and Ultrasound-Guided Intramyocardial Injections.** Data are accumulated from two independent experiments (total $n = 22$ mice). Adherent CSC-Luc2 cells were labeled in culture with 25 μg/mL Xenolight DiR fluorescent lipophilic membrane dye (PerkinElmer, Llantrisant, UK) for 40 min at 37 °C, then were dissociated in filter-sterilized 1× Hank's Balanced Salt Solution (HBSS), 10 mM HEPES, 30 mM taurine, 0.1 mg/mL liberase (Roche, West Sussex, UK) and 0.5 mg/mL DNase I (Roche, West Sussex, UK) at 37 °C for 5−10 min. After cells were removed from the tissue culture plastic, an equal volume of stopping buffer was added (20% (v/v) FBS, 1× HBSS, 10 mM HEPES, 30 mM taurine). Cells were harvested at 300*g* at 4 °C for 5 min and resuspended in DPBS. All starting cell populations had a viability >90%.

Mice were anaesthetised with 2.5% isoflurane in $O_2$, hair was removed from the injection sites, and the mice were laid supine with limbs attached to ECG electrodes. Hearts were imaged using a Vevo 2100 high-resolution ultrasound imaging system equipped with a 40 MHz transducer (FujiFilmVisualsonics, SonoSite, Toronto, Ontario, Canada). Using the parasternal short axis view 4 × 10 μL intramyocardial injections containing a total of 3.5 × $10^5$ CSC-Luc2 cells in either DPBS or encapsulated in 50% HBP containing 2 mM Gd(III)-HBP were made under ultrasound-guidance.[55] For hind limb injections, 100 μL containing 1.5 × $10^6$ CSC-Luc2 cells were injected intramuscularly using a 27G needle, either in DPBS or encapsulated in 100% and 50% HBP containing 2 mM Gd(III)-HBP.

**5.10. In Vivo Imaging.** Cardiac function was assessed just prior to and after intramyocardial injections using 2D ultrasound as above. Serial MRI analyses of mouse heart function were performed on days 1, 7, and 14. T1 mapping of the mouse hind limbs and chest were conducted on days 7 and 14 to determine the amount of hydrogel material remaining.

Grafted cell viability was assessed by serial bioluminescent imaging on days 0, 1, 3, 7, and 14, using a PhotonIMAGER Optima dynamic optical imaging system (Biospace Lab, Nesles la Vallée, France), 20 min after intraperitoneal administration of 10 μL of 30 mg/mL D-luciferin solution was injected per g of mouse body weight. Untransduced samples were used to subtract out background signal. For each animal, all subsequent data points were normalized to the initial day 0 luminescent signals.

**5.11. Statistical Analysis.** Data are reported as mean values ± standard deviation unless otherwise noted. One-or two-way analysis of variance with Bonferroni's correction was used for multiple comparisons. Student's two-tailed *t* test was used for pairwise comparisons. For serial analysis of cell engraftment, a Kruskal−Wallis H test and one-tailed Mann−Whitney U test were performed. $p < 0.05$ was considered significant.

## ■ ASSOCIATED CONTENT

### Supporting Information

The Supporting Information is available free of charge on the ACS Publications website at DOI: 10.1021/acscentsci.7b00039.

Supplemental figures containing mass spectra of synthesized peptides; chemical, degradation, and T1 mapping calibration of the Gd(III)-containing hydrogel; relative cell quantification method in metabolic assay; representative rheology sweeps of various hydrogel formulations; and cardiac function assessment of mice during in vivo study (PDF)

## ■ AUTHOR INFORMATION


### Corresponding Authors

*E-mail: m.d.schneider@imperial.ac.uk (M.D.S.).
*E-mail: m.stevens@imperial.ac.uk (M.M.S.).

### ORCID

Alessondra T. Speidel: 0000-0002-2576-2015
Molly M. Stevens: 0000-0002-7335-266X


### Author Contributions

L.W.C., D.J.S., and A.T.S. designed experiments. D.J.S. performed the intramyocardial and hind limb injections. D.J.S. and L.J. performed the MRI imaging and T1 analysis. M.A.P. prepared cell culture materials. M.N. provided the CSC. A.T.S. performed the remainder of the experiments, data analysis, and wrote the manuscript. D.J.S., L.W.C., M.D.S., and M.M.S. provided scientific guidance, supervised, and edited the manuscript.

### Notes

All animal work was performed in accordance with the UK Animals (Scientific Procedures) Act, 1986 and associated guidelines, EU Directive 2010/63/EU for animal experiments. The authors declare no competing financial interest.
Raw data is available upon request from m.stevens@imperial.ac.uk.

## ■ ACKNOWLEDGMENTS

This research was supported by the British Heart Foundation (CH/08/002/25297, RE/08/002/23906, RE/13/4/30184, RG/15/1/31165, RM/13/1/30157: MDS; FS/15/33/31608: DJS), the Medical Research Council (G0901467: MDS), the ERC Seventh Framework Programme Consolidator "Naturale CG" Grant (616417: MMS), the Wellcome Trust Senior Investigator Award (098411/Z/12/Z: MMS), the Marshall Aid Commemoration Commission (ATS), and the Rosetrees Trust



DOI: 10.1021/acscentsci.7b00039
ACS Cent. Sci. 2017, 3, 338−348

(ATS). The authors would like to thank Dr. Lisa Haigh for her aid in mass spectrometry data acquisition.

## REFERENCES

(1) Pavo, N.; Charwat, S.; Nyolczas, N.; Jakab, A.; Murlasits, Z.; Bergler-Klein, J.; Nikfardjam, M.; Benedek, I.; Benedek, T.; Pavo, I. J.; et al. Cell Therapy for Human Ischemic Heart Diseases: Critical Review and Summary of the Clinical Experiences. *J. Mol. Cell. Cardiol.* **2014**, *75*, 12−24.

(2) Makkar, R. R.; Smith, R. R.; Cheng, K.; Malliaras, K.; Thomson, L. E. J.; Berman, D.; Czer, L. S. C.; Marbán, L.; Mendizabal, A.; Johnston, P. V.; et al. Intracoronary Cardiosphere-Derived Cells for Heart Regeneration after Myocardial Infarction (CADUCEUS): A Prospective, Randomised Phase 1 Trial. *Lancet* **2012**, *379*, 895−904.

(3) de Jong, R.; Houtgraaf, J. H.; Samiei, S.; Boersma, E.; Duckers, H. J. Intracoronary Stem Cell Infusion after Acute Myocardial Infarction: A Meta-Analysis and Update on Clinical Trials. *Circ.: Cardiovasc. Interventions* **2014**, *7*, 156−167.

(4) Gyöngyösi, M.; Wojakowski, W.; Lemarchand, P.; Lunde, K.; Tendera, M.; Bartunek, J.; Marban, E.; Assmus, B.; Henry, T. D.; Traverse, J. H.; et al. Meta-Analysis of Cell-Based CaRdiac stUdiEs (ACCRUE) in Patients with Acute Myocardial Infarction Based on Individual Patient Data. *Circ. Res.* **2015**, *116*, 1346−1360.

(5) Sanganalmath, S. K.; Bolli, R. Cell Therapy for Heart Failure: A Comprehensive Overview of Experimental and Clinical Studies, Current Challenges, and Future Directions. *Circ. Res.* **2013**, *113*, 810−834.

(6) Noseda, M.; Harada, M.; McSweeney, S.; Leja, T.; Belian, E.; Stuckey, D. J.; Abreu Paiva, M. S.; Habib, J.; Macaulay, I.; de Smith, A. J.; et al. PDGFR$\alpha$ Demarcates the Cardiogenic Clonogenic Sca1+ Stem/progenitor Cell in Adult Murine Myocardium. *Nat. Commun.* **2015**, *6*, 6930.

(7) Assmus, B.; Walter, D. H.; Seeger, F. H.; Leistner, D. M.; Steiner, J.; Ziegler, I.; Lutz, A.; Khaled, W.; Klotsche, J.; Tonn, T.; et al. Effect of Shock Wave-Facilitated Intracoronary Cell Therapy on LVEF in Patients with Chronic Heart Failure: The CELLWAVE Randomized Clinical Trial. *JAMA* **2013**, *309*, 1622−1631.

(8) Tang, Y. L.; Zhu, W.; Cheng, M.; Chen, L.; Zhang, J.; Sun, T.; Kishore, R.; Phillips, M. I.; Losordo, D. W.; Qin, G. Hypoxic Preconditioning Enhances the Benefit of Cardiac Progenitor Cell Therapy for Treatment of Myocardial Infarction by Inducing CXCR4 Expression. *Circ. Res.* **2009**, *104*, 1209−1216.

(9) Dai, W.; Hale, S. L.; Kay, G. L.; Jyrala, A. J.; Kloner, R. A. Delivering Stem Cells to the Heart in a Collagen Matrix Reduces Relocation of Cells to Other Organs as Assessed by Nanoparticle Technology. *Regener. Med.* **2009**, *4*, 387−395.

(10) Yu, J.; Du, K. T.; Fang, Q.; Gu, Y.; Mihardja, S. S.; Sievers, R. E.; Wu, J. C.; Lee, R. J. The Use of Human Mesenchymal Stem Cells Encapsulated in RGD Modified Alginate Microspheres in the Repair of Myocardial Infarction in the Rat. *Biomaterials* **2010**, *31*, 7012−7020.

(11) Lu, W.-N.; Lü, S.-H.; Wang, H.-B.; Li, D.-X.; Duan, C.-M.; Liu, Z.-Q.; Hao, T.; He, W.-J.; Xu, B.; Fu, Q.; et al. Functional Improvement of Infarcted Heart by Co-Injection of Embryonic Stem Cells with Temperature-Responsive Chitosan Hydrogel. *Tissue Eng., Part A* **2009**, *15*, 1437−1447.

(12) Oberwallner, B.; Brodarac, A.; Choi, Y.-H.; Saric, T.; Anić, P.; Morawietz, L.; Stamm, C. Preparation of Cardiac Extracellular Matrix Scaffolds by Decellularization of Human Myocardium. *J. Biomed. Mater. Res., Part A* **2014**, *102*, 3263−3272.

(13) Christman, K. L.; Vardanian, A. J.; Fang, Q.; Sievers, R. E.; Fok, H. H.; Lee, R. J. Injectable Fibrin Scaffold Improves Cell Transplant Survival, Reduces Infarct Expansion, and Induces Neovasculature Formation in Ischemic Myocardium. *J. Am. Coll. Cardiol.* **2004**, *44*, 654−660.

(14) Huang, C.-C.; Wei, H.-J.; Yeh, Y.-C.; Wang, J.-J.; Lin, W.-W.; Lee, T.-Y.; Hwang, S.-M.; Choi, S.-W.; Xia, Y.; Chang, Y.; et al. Injectable PLGA Porous Beads Cellularized by hAFSCs for Cellular Cardiomyoplasty. *Biomaterials* **2012**, *33*, 4069−4077.

(15) Miyagi, Y.; Zeng, F.; Huang, X.-P.; Foltz, W. D.; Wu, J.; Mihic, A.; Yau, T. M.; Weisel, R. D.; Li, R.-K. Surgical Ventricular Restoration with a Cell- and Cytokine-Seeded Biodegradable Scaffold. *Biomaterials* **2010**, *31*, 7684−7694.

(16) Li, X.; Zhou, J.; Liu, Z.; Chen, J.; Lü, S.; Sun, H.; Li, J.; Lin, Q.; Yang, B.; Duan, C.; et al. A PNIPAAm-Based Thermosensitive Hydrogel Containing SWCNTs for Stem Cell Transplantation in Myocardial Repair. *Biomaterials* **2014**, *35*, 5679−5688.

(17) Zhang, S.; Holmes, T. C.; DiPersio, C. M.; Hynes, R. O.; Su, X.; Rich, A. Self-Complementary Oligopeptide Matrices Support Mammalian Cell Attachment. *Biomaterials* **1995**, *16*, 1385−1393.

(18) Reis, L. A.; Chiu, L. L. Y.; Feric, N.; Fu, L.; Radisic, M. Biomaterials in Myocardial Tissue Engineering. *J. Tissue Eng. Regener. Med.* **2016**, *10*, 11−28.

(19) Ripa, R. S.; Jørgensen, E.; Wang, Y.; Thune, J. J.; Nilsson, J. C.; Søndergaard, L.; Johnsen, H. E.; Køber, L.; Grande, P.; Kastrup, J. Stem Cell Mobilization Induced by Subcutaneous Granulocyte-Colony Stimulating Factor to Improve Cardiac Regeneration after Acute ST-Elevation Myocardial Infarction: Result of the Double-Blind, Randomized, Placebo-Controlled Stem Cells in Myocardial Infarction (STEMMI) Trial. *Circulation* **2006**, *113*, 1983−1992.

(20) Beohar, N.; Rapp, J.; Pandya, S.; Losordo, D. W. Rebuilding the Damaged Heart: The Potential of Cytokines and Growth Factors in the Treatment of Ischemic Heart Disease. *J. Am. Coll. Cardiol.* **2010**, *56*, 1287−1297.

(21) Lai, C. Y.; Wu, P. J.; Roffler, S. R.; Lee, S. T.; Hwang, S. M.; Wang, S. S.; Wang, K.; Hsieh, P. C. H. Clearance Kinetics of Biomaterials Affects Stem Cell Retention and Therapeutic Efficacy. *Biomacromolecules* **2014**, *15*, 564−573.

(22) Dubois, G.; Segers, V. F. M.; Bellamy, V.; Sabbah, L.; Peyrard, S.; Bruneval, P.; Hagège, A. A.; Lee, R. T.; Menasché, P. Self-Assembling Peptide Nanofibers and Skeletal Myoblast Transplantation in Infarcted Myocardium. *J. Biomed. Mater. Res., Part B* **2008**, *87*, 222−228.

(23) Artzi, N.; Oliva, N.; Puron, C.; Shitreet, S.; Artzi, S.; bon Ramos, A.; Groothuis, A.; Sahagian, G.; Edelman, E. R. In Vivo and in Vitro Tracking of Erosion in Biodegradable Materials Using Non-Invasive Fluorescence Imaging. *Nat. Mater.* **2011**, *10*, 704−709.

(24) Kim, K.; Jeong, C. G.; Hollister, S. J. Non-Invasive Monitoring of Tissue Scaffold Degradation Using Ultrasound Elasticity Imaging. *Acta Biomater.* **2008**, *4*, 783−790.

(25) Liang, X.; Graf, B. W.; Boppart, S. A. Imaging Engineered Tissues Using Structural and Functional Optical Coherence Tomography. *J. Biophotonics* **2009**, *2*, 643−655.

(26) Dorsey, S. M.; McGarvey, J. R.; Wang, H.; Nikou, A.; Arama, L.; Koomalsingh, K. J.; Kondo, N.; Gorman, J. H.; Pilla, J. J.; Gorman, R. C.; et al. MRI Evaluation of Injectable Hyaluronic Acid-Based Hydrogel Therapy to Limit Ventricular Remodeling after Myocardial Infarction. *Biomaterials* **2015**, *69*, 65−75.

(27) Reiss, S.; Krafft, A. J.; Zehender, M.; Heidt, T.; Pfannebecker, T.; Bode, C.; Bock, M.; von Zur Muhlen, C. Magnetic Resonance Imaging of Bioresorbable Vascular Scaffolds: Potential Approach for Noninvasive Evaluation of Coronary Patency. *Circ.: Cardiovasc. Interventions* **2015**, *8*, e002388.

(28) Stuckey, D. J.; Carr, C. A.; Martin-Rendon, E.; Tyler, D. J.; Willmott, C.; Cassidy, P. J.; Hale, S. J. M.; Schneider, J. E.; Tatton, L.; Harding, S. E.; et al. Iron Particles for Noninvasive Monitoring of Bone Marrow Stromal Cell Engraftment Into, and Isolation of Viable Engrafted Donor Cells From, the Heart. *Stem Cells* **2006**, *24*, 1968−1975.

(29) Doyle, B.; Kemp, B. J.; Chareonthaitawee, P.; Reed, C.; Schmeckpeper, J.; Sorajja, P.; Russell, S.; Araoz, P.; Riederer, S. J.; Caplice, N. M. Dynamic Tracking During Intracoronary Injection of 18F-FDG-Labeled Progenitor Cell Therapy for Acute Myocardial Infarction. *J. Nucl. Med.* **2007**, *48*, 1708−1714.

(30) Willmann, J. K.; Paulmurugan, R.; Rodriguez-Porcel, M.; Stein, W.; Brinton, T. J.; Connolly, A. J.; Nielsen, C. H.; Lutz, A. M.; Lyons, J.; Ikeno, F.; et al. Imaging Gene Expression in Human Mesenchymal



DOI: 10.1021/acscentsci.7b00039
*ACS Cent. Sci.* 2017, 3, 338−348

Stem Cells: From Small to Large Animals. *Radiology* **2009**, *252*, 117−127.
(31) Coombe, D. R.; Nakhoul, a M.; Stevenson, S. M.; Peroni, S. E.; Sanderson, C. J. Expressed Luciferase Viability Assay (ELVA) for the Measurement of Cell Growth and Viability. *J. Immunol. Methods* **1998**, *215*, 145−150.
(32) Roura, S.; Gálvez-Montón, C.; Bayes-Genis, A. Bioluminescence Imaging: A Shining Future for Cardiac Regeneration. *J. Cell. Mol. Med.* **2013**, *17*, 693−703.
(33) Pascual-Gil, S.; Garbayo, E.; Díaz-Herráez, P.; Prosper, F.; Blanco-Prieto, M. J. Heart Regeneration after Miocardial Infarction Using Synthetic Biomaterials. *J. Controlled Release* **2015**, *203*, 23−38.
(34) Cardin, a. D.; Weintraub, H. J. Molecular Modeling of Protein-Glycosaminoglycan Interactions. *Arterioscler., Thromb., Vasc. Biol.* **1989**, *9*, 21−32.
(35) Chow, L. W.; Bitton, R.; Webber, M. J.; Carvajal, D.; Shull, K. R.; Sharma, A. K.; Stupp, S. I. A Bioactive Self-Assembled Membrane to Promote Angiogenesis. *Biomaterials* **2011**, *32*, 1574−1582.
(36) Kalcioglu, Z. I.; Mrozek, R. A.; Mahmoodian, R.; VanLandingham, M. R.; Lenhart, J. L.; Van Vliet, K. J. Tunable Mechanical Behavior of Synthetic Organogels as Biofidelic Tissue Simulants. *J. Biomech.* **2013**, *46*, 1583−1591.
(37) Bauer, M.; Cheng, S.; Jain, M.; Ngoy, S.; Theodoropoulos, C.; Trujillo, A.; Lin, F.-C.; Liao, R. Echocardiographic Speckle-Tracking Based Strain Imaging for Rapid Cardiovascular Phenotyping in Mice. *Circ. Res.* **2011**, *108*, 908−916.
(38) Ruzsics, B.; Surányi, P.; Kiss, P.; Brott, B. C.; Litovsky, S.; Denney, T. S.; Aban, I.; Lloyd, S. G.; Simor, T.; Elgavish, G. A.; et al. Myocardial Strain in Sub-Acute Peri-Infarct Myocardium. *Int. J. Cardiovasc. Imaging* **2009**, *25*, 151−159.
(39) Wong, D. T. L.; Weightman, M. J.; Baumert, M.; Tayeb, H.; Richardson, J. D.; Puri, R.; Bertaso, A. G.; Roberts-Thomson, K. C.; Sanders, P.; Worthley, M. I.; et al. Electro-Mechanical Characteristics of Myocardial Infarction Border Zones and Ventricular Arrhythmic Risk: Novel Insights from Grid-Tagged Cardiac Magnetic Resonance Imaging. *Eur. Radiol.* **2012**, *22*, 1651−1658.
(40) Sun, N.; Lee, A.; Wu, J. C. Long Term Non-Invasive Imaging of Embryonic Stem Cells Using Reporter Genes. *Nat. Protoc.* **2009**, *4*, 1192−1201.
(41) Park, J.-A.; Lee, Y. J.; Ko, I. O.; Kim, T.-J.; Chang, Y.; Lim, S. M.; Kim, K. M.; Kim, J. Y. Improved Tumor-Targeting MRI Contrast Agents: Gd(DOTA) Conjugates of a Cycloalkane-Based RGD Peptide. *Biochem. Biophys. Res. Commun.* **2014**, *455*, 246−250.
(42) Berdichevski, A.; Shachaf, Y.; Wechsler, R.; Seliktar, D. Protein Composition Alters in Vivo Resorption of PEG-Based Hydrogels as Monitored by Contrast-Enhanced MRI. *Biomaterials* **2015**, *42*, 1−10.
(43) Rane, A. a; Christman, K. L. Biomaterials for the Treatment of Myocardial Infarction: A 5-Year Update. *J. Am. Coll. Cardiol.* **2011**, *58*, 2615−2629.
(44) Browning, M. B.; Cereceres, S. N.; Luong, P. T.; Cosgriff-Hernandez, E. M. Determination of the in Vivo Degradation Mechanism of PEGDA Hydrogels. *J. Biomed. Mater. Res., Part A* **2014**, *102*, 4244−4251.
(45) Elbert, D. L.; Pratt, A. B.; Lutolf, M. P.; Halstenberg, S.; Hubbell, J. A. Protein Delivery from Materials Formed by Self-Selective Conjugate Addition Reactions. *J. Controlled Release* **2001**, *76*, 11−25.
(46) Guo, H.; Cui, G.; Yang, J.; Wang, C.; Zhu, J.; Zhang, L.; Jiang, J.; Shao, S. Sustained Delivery of VEGF from Designer Self-Assembling Peptides Improves Cardiac Function after Myocardial Infarction. *Biochem. Biophys. Res. Commun.* **2012**, *424*, 105−111.
(47) Chow, L. W.; Wang, L.-J.; Kaufman, D. B.; Stupp, S. I. Self-Assembling Nanostructures to Deliver Angiogenic Factors to Pancreatic Islets. *Biomaterials* **2010**, *31*, 6154−6161.
(48) Hastings, C. L.; Roche, E. T.; Ruiz-Hernandez, E.; Schenke-Layland, K.; Walsh, C. J.; Duffy, G. P. Drug and Cell Delivery for Cardiac Regeneration. *Adv. Drug Delivery Rev.* **2015**, *84*, 85−106.
(49) Habib, M.; Shapira-Schweitzer, K.; Caspi, O.; Gepstein, A.; Arbel, G.; Aronson, D.; Seliktar, D.; Gepstein, L. A Combined Cell Therapy and in-Situ Tissue-Engineering Approach for Myocardial Repair. *Biomaterials* **2011**, *32*, 7514−7523.
(50) Stuckey, D. J.; Sc, B.; Phil, D.; Ishii, H.; Ph, D.; Chen, Q.; Boccaccini, A. R.; Hansen, U.; Carr, C. A.; Roether, J. A.; et al. Magnetic Resonance Imaging Evaluation of Remodeling by Cardiac Elastomeric Tissue Scaffold Biomaterials in a Rat Model of Myocardial Infarction. *Tissue Eng., Part A* **2010**, *16*, 3395−3402.
(51) Dorsey, S. M.; Haris, M.; Singh, A.; Witschey, W. R. T.; Rodell, C. B.; Kogan, F.; Reddy, R.; Burdick, J. A. Visualization of Injectable Hydrogels Using Chemical Exchange Saturation Transfer MRI. *ACS Biomater. Sci. Eng.* **2015**, *1*, 227−237.
(52) Lutolf, M. P.; Tirelli, N.; Cerritelli, S.; Cavalli, L.; Hubbell, J. a. Systematic Modulation of Michael-Type Reactivity of Thiols through the Use of Charged Amino Acids. *Bioconjugate Chem.* **2001**, *12*, 1051−1056.
(53) Mawad, D.; Martens, P. J.; Odell, R. A.; Poole-Warren, L. A. The Effect of Redox Polymerisation on Degradation and Cell Responses to Poly (Vinyl Alcohol) Hydrogels. *Biomaterials* **2007**, *28*, 947−955.
(54) Stuckey, D. J.; McSweeney, S. J.; Thin, M. Z.; Habib, J.; Price, A. N.; Fiedler, L. R.; Gsell, W.; Prasad, S. K.; Schneider, M. D. $T_1$ Mapping Detects Pharmacological Retardation of Diffuse Cardiac Fibrosis in Mouse Pressure-Overload Hypertrophy. *Circ. Cardiovasc. Imaging* **2014**, *7*, 240−249.
(55) Springer, M. L.; Sievers, R. E.; Viswanathan, M. N.; Yee, M. S.; Foster, E.; Grossman, W.; Yeghiazarians, Y. Closed-Chest Cell Injections into Mouse Myocardium Guided by High-Resolution Echocardiography. *Am. J. Physiol. Heart Circ. Physiol.* **2005**, *289*, H1307−H1314.


DOI: 10.1021/acscentsci.7b00039
*ACS Cent. Sci.* 2017, 3, 338−348